

Inhibition of solute crystallisation in aqueous $\text{H}^+ - \text{NH}_4^+ - \text{SO}_4^{2-} - \text{H}_2\text{O}$ droplets

Benjamin J. Murray^{*ab} and Allan K. Bertram^a

Received 8th February 2008, Accepted 17th March 2008

First published as an Advance Article on the web 21st April 2008

DOI: 10.1039/b802216j

Ice clouds in the Earth's upper troposphere can form *via* homogeneous nucleation of ice in aqueous droplets. In this study we investigate the crystallisation, or lack of crystallisation, of the solute phase and ice in aqueous $(\text{NH}_4)_3\text{H}(\text{SO}_4)_2/\text{H}_2\text{O}$ and $\text{NH}_4\text{HSO}_4/\text{H}_2\text{O}$ droplets. This is done using *in situ* X-ray diffraction of emulsified solution droplets mounted on a cold stage. From the diffraction patterns we are able to identify the phases of crystalline solute and ice that form after homogeneous freezing in micrometer sized droplets. An important finding from this study is that crystallisation of the solute does not always occur, even when crystallisation is strongly thermodynamically favoured. The nucleation and growth of solute phase crystals becomes inhibited since the viscosity of the aqueous brine most likely increases dramatically as the brine concentration increases and temperature decreases. If ice nucleates below a threshold freezing temperature, the brine appears to rapidly become so viscous that solute crystallisation is inhibited. This threshold temperature is 192 K and 180 K, in $(\text{NH}_4)_3\text{H}(\text{SO}_4)_2$ and NH_4HSO_4 , respectively. We also speculate that the formation of cubic ice within a highly viscous brine blocks the solvent mediated cubic to hexagonal phase transformation, thus stabilising the metastable cubic ice in the most concentrated solution droplets.

Introduction

Ice clouds that occur in the Earth's upper troposphere (UT, 12–18 km) have been the focus of intense research during the past few decades.^{1,2} These clouds play an important role in the Earth's climate by scattering and absorbing radiation, although their present and future net climatic impact remains uncertain.³ In addition, the formation and precipitation of ice clouds influences both the distribution of water vapour in the UT as well as the amount of water vapour that enters the stratosphere, where it may have important consequences for polar stratospheric ozone.^{4,5}

A significant mechanism of ice cloud formation in the UT and tropopause region is thought to be homogeneous freezing of submicron aqueous droplets.⁶ Recently it was shown that the metastable cubic crystalline phase of ice (ice I_c) was produced when aqueous $(\text{NH}_4)_3\text{H}(\text{SO}_4)_2$, $(\text{NH}_4)_2\text{SO}_4$, NaCl and HNO_3 solution droplets froze homogeneously under conditions that are relevant for the UT and tropopause.⁷ Grothe *et al.*⁸ demonstrated that cubic ice crystallised from amorphous HNO_3 -water samples. Until recently, it was often assumed that only the stable hexagonal phase (ice I_h) would form under conditions relevant for the UT and tropopause.⁹ This is particularly relevant since cubic ice has a larger vapour pressure than hexagonal ice¹⁰ and may therefore influence cloud properties.^{7,11}

In an even more recent study, we investigated in detail the formation of cubic ice in $(\text{NH}_4)_3\text{H}(\text{SO}_4)_2/\text{H}_2\text{O}$ and $\text{NH}_4\text{HSO}_4/\text{H}_2\text{O}$ droplets.¹² It was shown that the phase of ice that forms strongly depends on the type of solute. Droplets of aqueous $(\text{NH}_4)_3\text{H}(\text{SO}_4)_2$ freeze dominantly to cubic ice over a range of temperatures relevant for the UT and tropopause (typically $> 186 \text{ K}^{13}$); whereas aqueous NH_4HSO_4 droplets freeze dominantly to the stable ice I_h at temperatures typical of the UT and tropopause region. However, a detailed explanation for the observed trends was not discussed. In this study we suggest that the crystallisation of the solute phase and the nature of the brine strongly influence the phase of ice that forms.

When ice crystallises in a solution droplet, solute ions are rejected to form aqueous brine from which crystalline solute phases can form. However, in our previous X-ray diffraction (XRD) studies^{7,12,14,15} we focused exclusively on the crystallisation of ice. In this paper we extend our previous work and explore the crystallisation of the solute phases in droplets where ice nucleated homogeneously. This has only received minimal attention in the past.^{16–19} In fact, there has been no systematic investigation of solute crystallisation after ice crystallisation as a function of droplet size, solute concentration and solute type.

It is often assumed that the solute phase crystallises immediately after or during ice formation if it is thermodynamically viable for it to do so. However, we show here that solute crystallisation does not always take place and may not occur in many atmospheric droplets. This is important because several studies suggest solute crystallisation subsequent to ice crystallisation may be an important mechanism for producing crystalline salt particles which may act as an ice nuclei in

^a Department of Chemistry, University of British Columbia, 2036 Main Mall Vancouver, British Columbia, Canada V6T 1Z1

^b School of Chemistry, University of Leeds, Woodhouse Lane, Leeds, UK LS2 9JT

subsequent cloud cycles, thereby influencing cloud properties.^{18–23} It is shown here that the solute phase may not crystallise in atmospheric droplets and therefore this mechanism may not be important.

There have been several investigations of the solute crystalline phases using bulk samples or thin films, where nucleation most likely occurred heterogeneously, in the $\text{H}^+ - \text{NH}_4^+ - \text{SO}_4^{2-} - \text{H}_2\text{O}$ system;^{24–27} these experiments were ideally suited for mapping out the equilibrium phase changes. However, in order to investigate kinetically controlled phase changes of atmospheric relevance, such as freezing or brine crystallisation, small droplets are required. Hence, in this study we investigate the crystallisation of micrometer sized droplets rather than bulk samples.

Our investigation is limited to a detailed study of $(\text{NH}_4)_3\text{H}(\text{SO}_4)_2/\text{H}_2\text{O}$ and $\text{NH}_4\text{HSO}_4/\text{H}_2\text{O}$ solution droplets. Solutions with these ammonium to sulfate ratios (ASR = 1.5 and 1, respectively) were chosen because it has been shown that they exhibited strongly contrasting behaviour.¹² The solutes $(\text{NH}_4)_3\text{H}(\text{SO}_4)_2$ and NH_4HSO_4 are referred to as LET and AHS for the remainder of this paper; indicating that the overall stoichiometry of the solute in the droplets corresponds to letovicite and ammonium bisulfate, respectively.

This paper is organised as follows: First, we identify the solute phases that form when LET and AHS solution droplets crystallise from the diffraction patterns. This is the first time the solute phase(s) have been measured and identified after freezing in micron sized solution droplets. Second, we investigate the temperatures at which the solute phases crystallise in the solution droplets after ice crystallisation. Third, we investigate the effect of solution concentration on crystallisation of the solute. In this section we show that the solute phases do not crystallise in the most concentrated solutions after ice nucleation. Fourth, we investigated the effect of droplet size on the crystallisation of the solute. The effect of particle size on crystallisation of the solute has not been investigated previously. This information is needed to extrapolate the measurements in the laboratory to atmospheric conditions and we show that the solute does not crystallise efficiently in very small droplets. Fifth, a possible explanation of previous cubic ice results (strong dependence on the ammonium to sulfate ratio) is presented¹² based on the solute crystallisation results. This explanation involves a solvent-mediated phase transition. In addition, the atmospheric implications of the results are briefly discussed.

Experimental

For these experiments, aqueous solution droplets in the micrometer size range were suspended in an oil matrix by emulsification. Phase transitions in the aqueous solution droplets were then monitored with X-ray diffraction. Two types of experiments were carried out. (1) The aqueous droplets were cooled at a rate of 10 K min^{-1} to 163 or 173 K, where the diffraction pattern between $2\theta = 19$ to 50° was measured and the crystalline phases that formed were determined from these patterns. (2) The temperature at which ice and the solute phases crystallised in the droplets as well as the melting temperatures of all the observed phases were determined by

either cooling or warming the droplets while monitoring a portion of the diffraction pattern. The two types of experiments were carried out concurrently.

The experimental technique has been described previously and will only be briefly summarized here.^{7,14} The X-ray diffractometer (Bruker D8 Discover) used in these experiments was configured in a standard Bragg-Brentano reflection geometry and was equipped with a $\text{Cu K}\alpha$ X-ray source. The data presented in this paper were measured with two different source and detector combinations. The results from both combinations are directly comparable and the specific instrumentation details are discussed elsewhere.^{7,14}

Aqueous solutions of an accurately known composition were prepared using pure water (distilled water further purified with a Millipore 18.2 M Ω system) and a gravimetric scale accurate to within 5 mg. Solid ammonium bisulfate was added to water to produce aqueous NH_4HSO_4 of concentrations between 0 at 39.2 wt% ($M_{\text{solute}}/[M_{\text{solute}} + M_{\text{solvent}}]$, where M is mass). Whereas $(\text{NH}_4)_3\text{H}(\text{SO}_4)_2$ solutions were prepared using two methods: (i) mixing ammonium sulfate with the correct amount of ammonium bisulfate or (ii) mixing ammonium sulfate with the correct amount of sulfuric acid. No difference was observed in the final diffraction patterns or phase change temperatures with solutions prepared using these two methods. Aqueous solutions of $(\text{NH}_4)_3\text{H}(\text{SO}_4)_2$ had concentrations of between 0 and 43.2 wt%. These solutions were then emulsified by mixing them with an oil phase. The oil phase consisted of mineral oil (paraffin oil, Fisher Scientific) and 10 wt% lanolin surfactant (Aldrich Chemical Company). This mixture was then mechanically agitated using a magnetic stirring bead until the droplets were of the desired size range. Smaller droplets were generated by mixing for longer. The droplet sizes were measured by optical microscopy and had volume median diameters of between 2 and $20 \mu\text{m}$ with geometric standard deviations between 1.3 and $1.8 \mu\text{m}$.

The emulsions containing droplets of the desired composition were placed in a cell within an X-ray diffraction chamber capable of low temperature measurements (TTK 450, Anton-Paar). It was previously shown that frozen droplets prepared in this manner exhibit no significant preferred orientation and that the diffraction patterns presented here are equivalent to powder patterns.¹⁴ It is thought that the nucleation and freezing process is not influenced by the oil or surfactant; this is discussed in detail later in the section titled ‘Ice freezing temperatures in the aqueous solutions’.

Results and discussion

Examples of the diffraction patterns of frozen LET, and AHS solution droplets are illustrated in Fig. 1. These patterns were measured after the emulsified droplets were cooled to either 173 K (or 163 K for the most concentrated AHS solution droplets) at a rate of 10 K min^{-1} . Inspection of Fig. 1 reveals that the patterns contain Bragg peaks from both ice and crystalline solute phases. The Bragg peaks exclusive to ice I_h are labelled “h” and the peaks common to both ice I_c and ice I_h are labelled “h+c”. There are no intense Bragg peaks unique to ice I_c . The peaks associated with the solute phases are labelled “S”, while those due to the aluminium base and

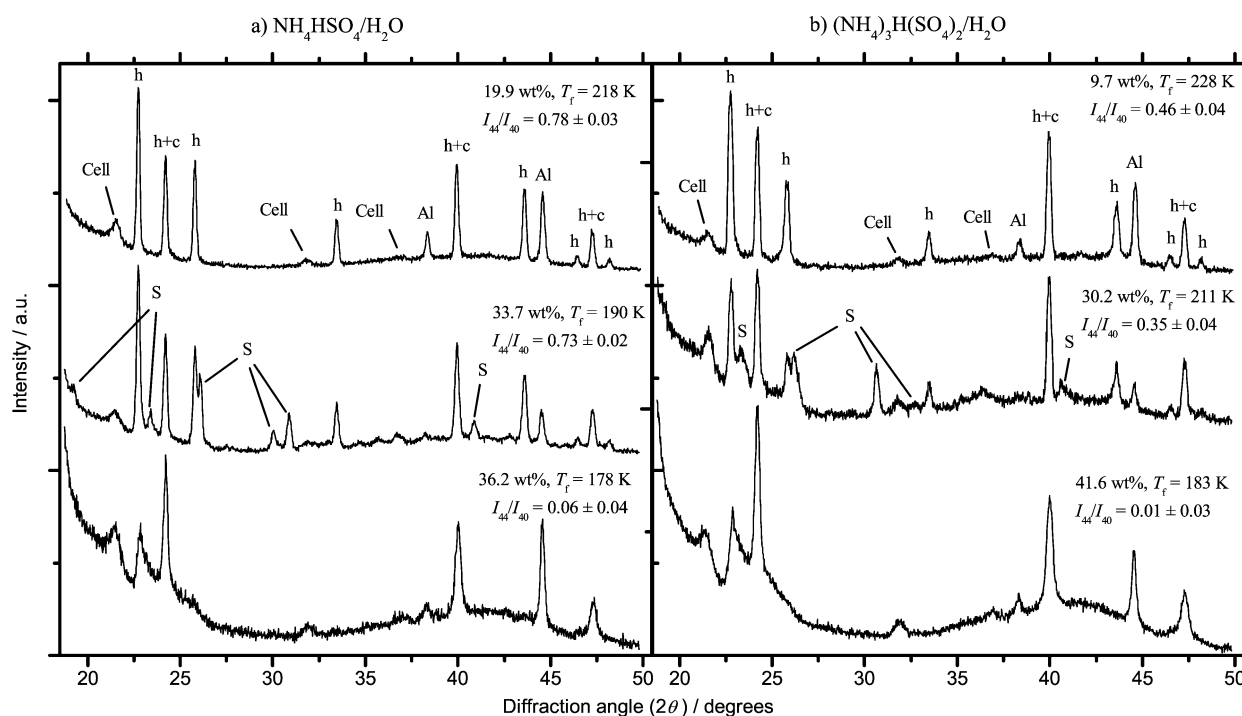


Fig. 1 Diffraction patterns of frozen (a) $(\text{NH}_4)_2\text{SO}_4/\text{H}_2\text{O}$ and (b) $(\text{NH}_4)_3\text{H}(\text{SO}_4)_2/\text{H}_2\text{O}$ droplets. These patterns were measured after the droplets had been cooled at a rate of 10 K min^{-1} to 173 K or 163 K. The mean freezing temperature, solute concentration and ratio of the hexagonal peak at 43.5° (I_{44}) to the common peak at 40° (I_{40}) are indicated for each pattern (see text for details). Bragg peaks associated with ice I_h are labelled “h”, while those common to both ice I_h and ice I_c are labelled “h + c”. Peaks associated with the solute phase are labelled “S” and those due to the cell construction materials and the aluminium base are labelled “Cell” and “Al”, respectively.

the cell construction materials are labelled “Al” and “Cell”, respectively. The underlying background on which the reflections from ice and the solute phase are superimposed is largely due to diffraction from the amorphous oil phase. The diffraction patterns illustrated in Fig. 1 show a great deal of variability depending on the solute and also on the concentration of the solution droplets. This is explored in detail below.

Identification of the crystalline solute phases

In the first part of this study we focused on identifying the crystalline solute phases that precipitated after ice nucleation in the aqueous droplets.

Diffraction patterns of frozen aqueous LET droplets. The aerosol inorganic model (AIM) predicts that crystalline letovicite ($(\text{NH}_4)_3\text{H}(\text{SO}_4)_2$) and ice are the thermodynamically stable phases that form at low temperatures in our LET solution droplets. Letovicite and ice have been identified experimentally in the past,^{25,28} but these previous studies were unable to identify the exact phase of letovicite. There are several known phases of letovicite,²⁹ each with a distinct crystal structure.³⁰ In a dielectric study Gesi²⁹ found Letovicite II formed at room temperature, whereas between 141 and 265 K Gesi identified letovicite III. In Fig. 2, a diffraction pattern of frozen 39.9 wt% LET droplets is compared to the patterns of letovicite II and III calculated with the Powder Cell programme³¹ and structural data from Dominiak *et al.*³⁰ Inspection of Fig. 2 reveals that several of the peaks in the calculated letovicite III pattern are absent in the experimental pattern, most notably those at $2\theta = 22$ and 28° ; whereas the

calculated pattern for letovicite II is consistent with the position and intensity of the experimental solute phase peaks. This shows that letovicite II formed in the aqueous droplets rather than the expected letovicite III.^{28–30} Also, note that the diffraction patterns for other crystalline salts (such as

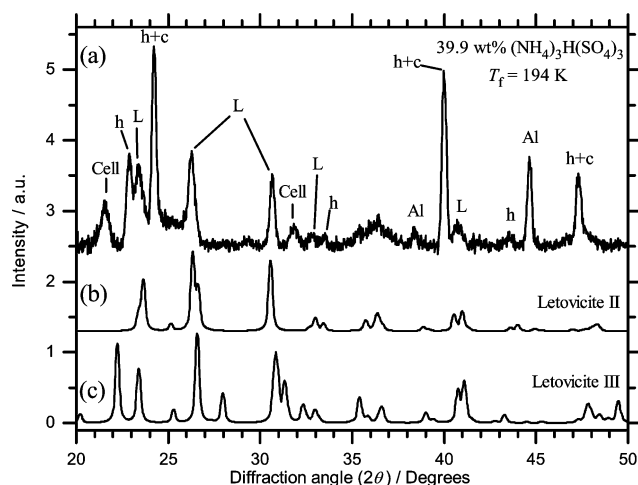


Fig. 2 Comparison of the diffraction pattern of frozen 39.9 wt% LET solution droplets (a), with the patterns of letovicite II (b) and letovicite III (c) calculated from structural data recorded in ref. 30 using the Powder Cell programme.³¹ Peaks common to both ice I_c and ice I_h are labelled “h + c” and peaks exclusive to ice I_h are labelled “h”. Peaks due to the cell construction materials are labelled “cell” and those due to the aluminium base are labelled “Al”. Peaks identified as those from crystalline letovicite are labelled “L”.

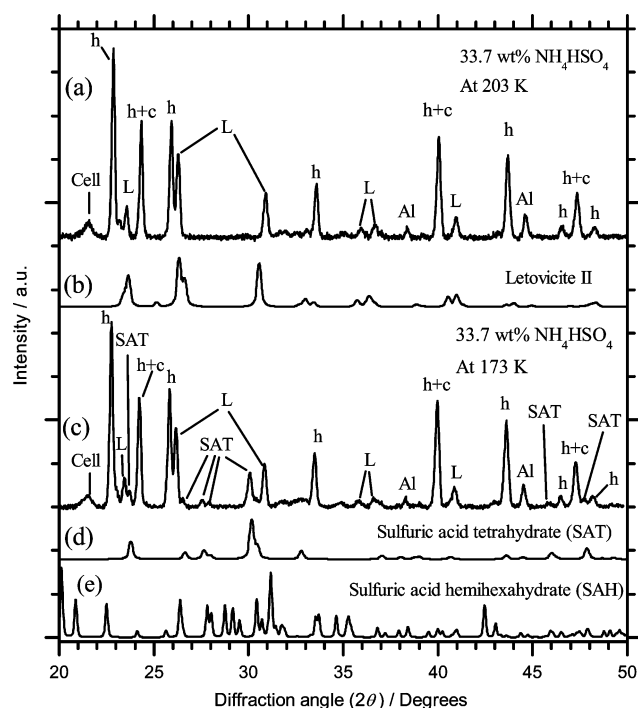


Fig. 3 Comparison of diffraction patterns of frozen 33.7 wt% AHS solution droplets with patterns of letovicite II (b), sulfuric acid tetrahydrate (SAT) (d), and sulfuric acid hemihexahydrate (e); calculated from data recorded in ref. 30, 33 and 34, respectively. Pattern a is that of 33.7 wt% AHS solution droplets which froze at 190 ± 5 K as they were cooled at 10 K min^{-1} and then warmed to 203 K, which is above the SAT eutectic temperature, but below the sulfuric acid hemihexahydrate eutectic (209 K³²). Pattern d is that of the same AHS solution droplets at 173 K before they were warmed to 203 K. The labelling is the same as in Fig. 2, but where ‘SAT’ indicates peaks that have been identified as SAT diffraction peaks.

crystalline ammonium sulfate, and bisulfate) are inconsistent with our measured diffraction patterns.)

Diffraction patterns of frozen aqueous AHS droplets. Patterns of frozen 33.7 wt% AHS droplets are shown in Fig. 3 at two different temperatures. Fig. 3c was produced by decreasing the temperature of these droplets, which froze at 190 ± 5 K, to 173 K and then recording the diffraction pattern. Then the pattern in Fig. 3a was recorded after warming this sample to 203 K. Examination of these two diffraction patterns reveals that a number of peaks present in the 173 K pattern are absent in the 203 K pattern; this indicates a phase change occurred between these temperatures. The phase change temperatures were recorded and are discussed later.

AIM³² predicts the stable phases that form at low temperatures are ice, letovicite and sulfuric acid hemihexahydrate (SAH) whereas previous experimental evidence based on calorimetry indicates sulfuric acid tetrahydrate (SAT), rather than SAH, form at low temperatures.^{24,25,27} In addition to the two experimental patterns we have shown patterns for Letovicite II, SAT, and SAH which were calculated from literature data.^{30,33,34} These ‘extra’ peaks in panel c are consistent with SAT and are inconsistent with the structure of SAH. As will be seen later the phase change temperatures are also consistent with SAT.

The remaining crystalline solute phase peaks which are present together with ice peaks at 203 K, broadly correspond to those in the pattern for letovicite II (pattern b). However, the match with the calculated pattern is not exact and in addition there are differences between the letovicite pattern in LET droplets and that in AHS droplets. In this case the identification of the letovicite phase is not as straightforward as it is in LET droplets. We have employed a computer programme to assess if these crystals are a distorted form of letovicite II or a different phase altogether. The computational technique widely used for these calculations is known as a Rietveld refinement,³⁵ and is a least-squared minimisation between the experimental pattern and a pattern generated from structural information which is adjusted to produce a best fit. We have used the refinement tool in the Powder Cell package.³¹

In a Rietveld refinement, it is assumed that the experimental pattern can be well represented by a linear combination of calculated patterns for the individual phases.³⁵ This is only true when the substances are well crystallised. The presence of stacking faults cannot be routinely accounted for in these refinements. However, we are fortunate in that the ice I_h that forms in the AHS droplets shown in Fig. 3 approximates well to stacking fault free ice I_h , hence a Rietveld refinement is possible. Such a refinement would not be meaningful for the LET droplets, because the ice that forms in them always contains significant stacking faults.⁷

We have taken literature data for the structures of Letovicite II,³⁰ SAT³³ and ice I_h ³⁶ as starting points in the refinement. The relative contribution of each phase, unit cell parameters, peak profiles, background and systematic diffraction angle offset have been fitted. The unique positions of the atoms and space groups have not been adjusted. The results of this refinement procedure for patterns in Fig. 3c are shown in Fig. 4 and the fitted unit cell parameters are listed in Table 1.

The quality of the fits indicated by the small residuals shows that it is possible to account for the peak positions and intensities. It is concluded here that ice I_h and SAT have structures almost identical to those in the literature, whereas the letovicite phase is a distorted form of letovicite II. We can be confident in this identification because relatively small adjustments to the unit cell dimensions were required to produce a fit (see Table 1) and the structure refined within the same space group ($C2/c$) and without altering the unique positions of the atoms. The reason for this distortion to the letovicite unit cell may be the acidic environment in which letovicite formed. It will be shown later in this paper that ice crystallises first, shortly followed by letovicite and then SAT crystallises at a much lower temperature. Hence, letovicite crystallises in an acidic environment in AHS, which could potentially cause some protonation of the letovicite which may have distorted its structure. It should also be noted that preferred orientation of the crystallites was not invoked to produce this fit, confirming that preferred orientation is not an issue in these experiments.

Melting temperatures in the aqueous LET and AHS systems. The melting temperatures of the frozen droplets were determined by continually monitoring a portion of the diffraction

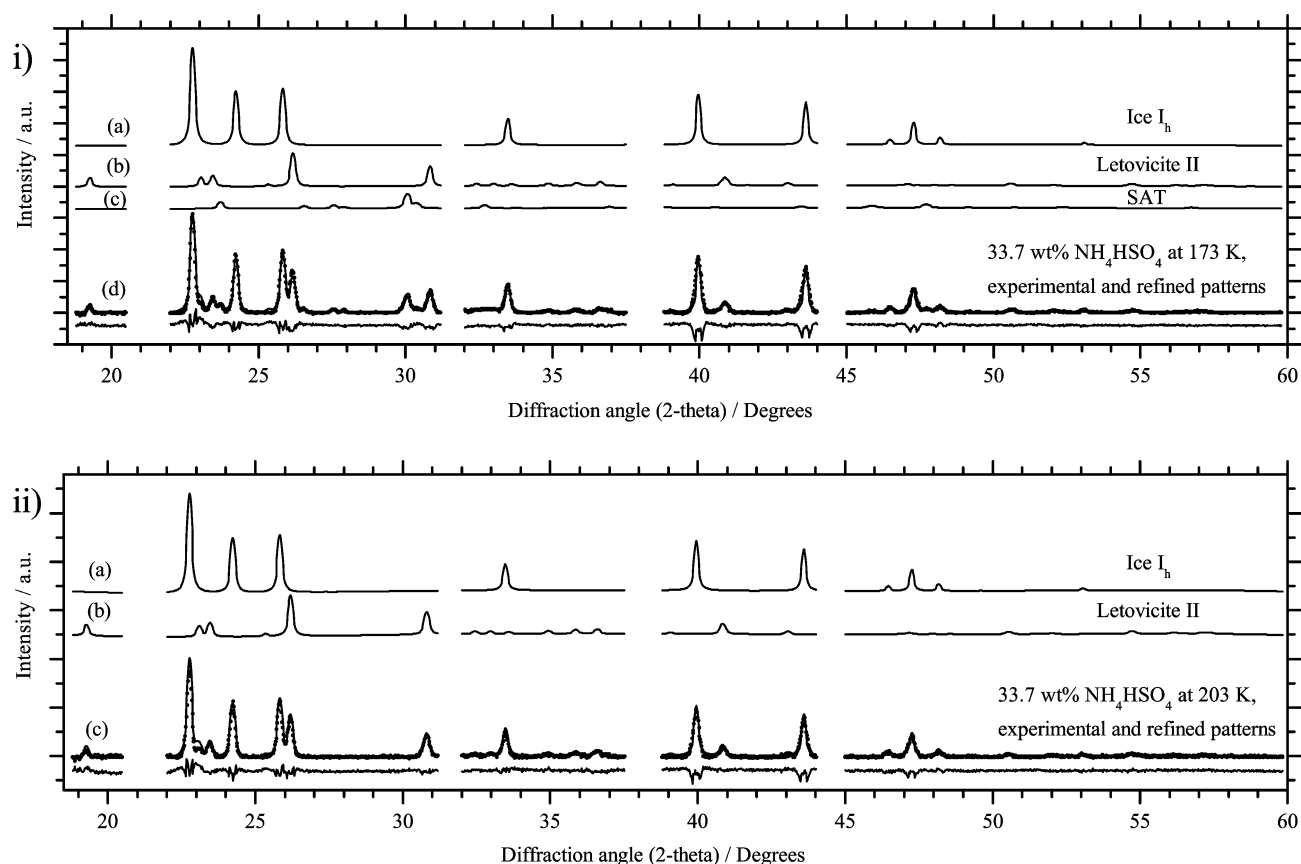


Fig. 4 Rietveld refinement fits to the experimental patterns (i) is the fit to the pattern of 33.7 wt% AHS droplets at 173 K (Fig. 3d) and (ii) the a fit to a pattern of the same droplets, which had been warmed to 203 K (Fig. 3b). The refined patterns of ice I_h , Letovicite II and SAT are also shown together with the fitted and experimental patterns in addition to the residuals.

pattern, which contained a pertinent peak (*i.e.* peaks that correspond to either ice or the crystalline solutes), as the droplets were warmed at a rate of 1 K min^{-1} (after being cooled to 173 or 163 K). The measured ice and solute phase melting temperatures for aqueous LET and AHS droplets are plotted in the phase diagrams in Fig. 5a and b. Our data are compared with the available literature data and also the predictions of AIM. In general, the agreement between data sets and model for the letovicite and ice melting points in both AHS and LET solutions is good. The exception is that of the

ice melting data for Imre *et al.*³⁷ in the AHS system; however, Chelf and Martin³⁸ suggest that there were errors in those measurements.

The agreement of experimental data with model predictions at lower temperature ($<215 \text{ K}$) is not as good. AIM predicts that the stable phases at low temperature are ice, letovicite and SAH (the SAH eutectic temperature is shown as a dotted line in Fig. 5b). The melting temperatures and the diffraction patterns suggest that SAT forms, rather than SAH. AIM predicts the formation of SAT if SAH is blocked; the SAT

Table 1 Literature and fitted unit cell parameters which were fitted in the Rietveld refinement in Fig. 4

Phase/fitted unit cell parameter	Literature	Fit to 173 K pattern	Fit to 203 K pattern
Letovicite II			
$a/\text{\AA}$	15.3900 ^a	15.7831	15.776
$b/\text{\AA}$	5.8480 ^a	5.7925	5.8010
$c/\text{\AA}$	10.1400 ^a	10.0479	10.0667
$\beta/^\circ$	101.810 ^a	102.065	102.244
Ice I_h			
$a/\text{\AA}$	4.5110 ^b	4.5100	4.5140
$b/\text{\AA}$	4.5110 ^b	4.5100	4.5140
$c/\text{\AA}$	7.3510 ^b	7.3433	7.3505
SAT			
$a/\text{\AA}$	7.4797 ^c	7.5036	NA
$b/\text{\AA}$	7.4797 ^c	7.5036	NA
$c/\text{\AA}$	6.3680 ^c	6.3913	NA

^a Dominiak *et al.*³⁰ ^b Goto *et al.*³⁶ ^c The 150 K data from Fortes *et al.*³³

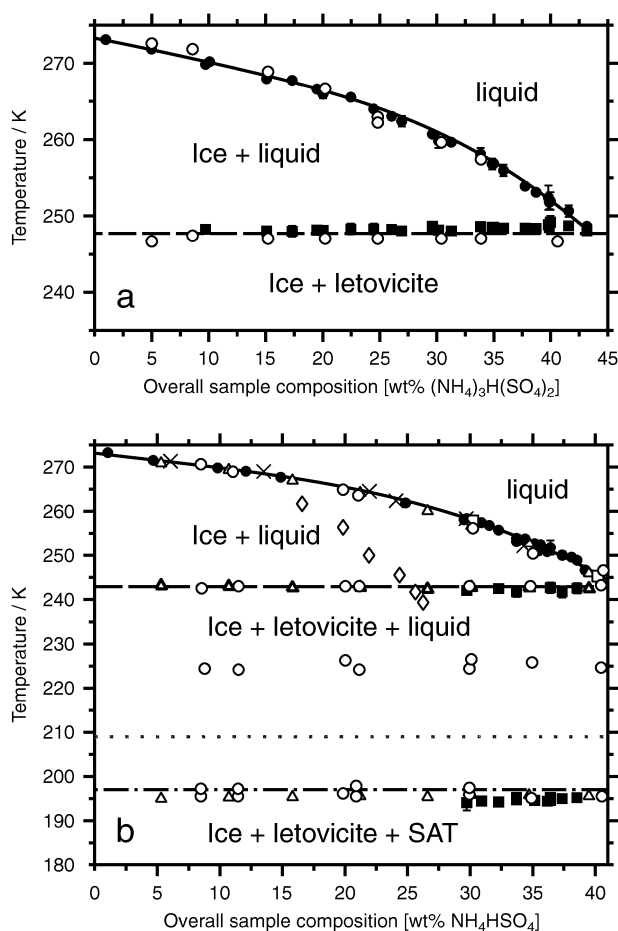


Fig. 5 Temperature–composition phase diagrams for (a) $(\text{NH}_4)_3\text{H}(\text{SO}_4)_2/\text{H}_2\text{O}$ and (b) $\text{NH}_4\text{HSO}_4/\text{H}_2\text{O}$. Temperatures at which we observed phase changes as droplets were warmed at 1 K min^{-1} are plotted as filled symbols; the uncertainty in temperature was typically smaller than the symbol size. Our measurements are superimposed on the equilibrium curves predicted by the Aerosol Inorganic Model.³² Our data is compared with literature data marked as circles,^{24,25} triangles,²⁷ crosses,³⁸ squares,⁶⁸ and diamonds.³⁷ In panels a and b, the equilibrium line of ice with liquid (solid) and that of ice + letovicite with liquid (dashed) are shown. In panel b, the equilibrium line of SAH + ice + letovicite with liquid (light dotted) and also the line for SAT + ice + letovicite in equilibrium with liquid (dot-dashed) are also shown.

eutectic is shown as a dot-dashed line in Fig. 5b. The melting temperatures recorded in thin films²⁴ and $3\ \mu\text{m}$ droplets (*i.e.* bulk),²⁷ which froze heterogeneously, also suggest SAT crystallised. It is unclear if there is an error in AIM, perhaps due to the extrapolations from high temperature thermodynamic data to these low temperatures employed in AIM,^{24,25,27} or if there is a large kinetic barrier to the formation of SAH. For a detailed discussion of the equilibrium phase diagrams of these systems see Beyer *et al.*²⁵ and Beyer and Bothe.²⁴

In a set of calorimetry and IR spectroscopy experiments Beyer and Bothe²⁴ found that ammonium bisulfate crystallised rapidly after SAT melted on warming and then converted to letovicite at 223.8 K . Our Rietveld refinement of a pattern of frozen droplets which had been cooled to 173 K and then warmed to 203 K , which is above the SAT eutectic, and held at

203 K for $\sim 30\text{ min}$ (Fig. 4ii) clearly shows ice and letovicite only. There is no evidence of the crystallisation of ammonium bisulfate. In our experiments the temperature was increased at a rate of 1 K min^{-1} across the SAT eutectic temperature, which is the same ramp rate employed by Beyer and Bothe.²⁴ The main difference between the experiments was that we used micrometer sized droplets while they used thin film samples. Beyer and Bothe note that when their film was ramped at 5 K min^{-1} , re-crystallisation is partially suppressed which indicates that nucleation becomes kinetically limited. Our results suggest that the nucleation rate of ammonium bisulfate in the SAT melt is very small in micron sized droplets.

Temperatures at which the solute phases and ice crystallised

After ice crystallised in the solution droplets, solute phase precipitation may become thermodynamically viable. However, crystallisation of the solute phase from a metastable brine may not occur for kinetic reasons. Using X-ray diffraction, we were able to determine the temperatures at which the various solutes crystallised in addition to the temperature at which ice crystallised by monitoring the intensity of a pertinent peak. Before we present the measurements of the temperatures at which the solute phases crystallised, we first present the temperatures at which ice formed in these solution droplets. The results for ice are needed so that we can make a comparison between the ice freezing temperatures and the solute crystallisation temperatures.

Ice freezing temperatures in the aqueous solutions. The temperature at which ice precipitated was determined by monitoring ice peaks as the emulsions were cooled at a rate of 10 K min^{-1} . The measured droplet freezing temperatures for aqueous LET and AHS droplets are plotted in Fig. 6a and b. In addition, we have also included a parameterisation of the ice melting temperatures for comparison. Unlike melting, freezing is a kinetically controlled nucleation process; hence it occurred over a range of temperature and at lower temperatures than melting. These freezing ranges are plotted in Fig. 6 with uncertainties in the onset and completion of freezing.

We argue that these freezing results correspond to homogeneous nucleation, rather than heterogeneous or a surface induced pseudo-heterogeneous nucleation pathway. The oil phase and surfactant did not significantly influence the nucleation mechanism for the following reasons. First, our freezing measurements for AHS droplets are compared with the experimental results of Koop *et al.* (dashed line in Fig. 6b),²⁷ where calorimetry was used to measure the temperature at which 50% of their $1\text{--}10\ \mu\text{m}$ emulsified droplets froze; the agreement with our measurements is good. Second, we determined freezing temperatures of $(\text{NH}_4)_2\text{SO}_4/\text{H}_2\text{O}$, $\text{NaCl}/\text{H}_2\text{O}$ and $\text{HNO}_3/\text{H}_2\text{O}$ droplets in previous measurements⁷ employing the same experimental technique used here (freezing data not shown). Our results are in good agreement with measurements of freezing in micron sized solution droplets recorded in the literature; including those with droplets falling through gas,³⁹ suspended on a surface⁴⁰ or suspended in an oil emulsion.^{16,40,41} Third, the freezing temperatures of pure water determined in our experiments¹⁴ are in good agreement with freezing temperatures of micron sized pure water droplets

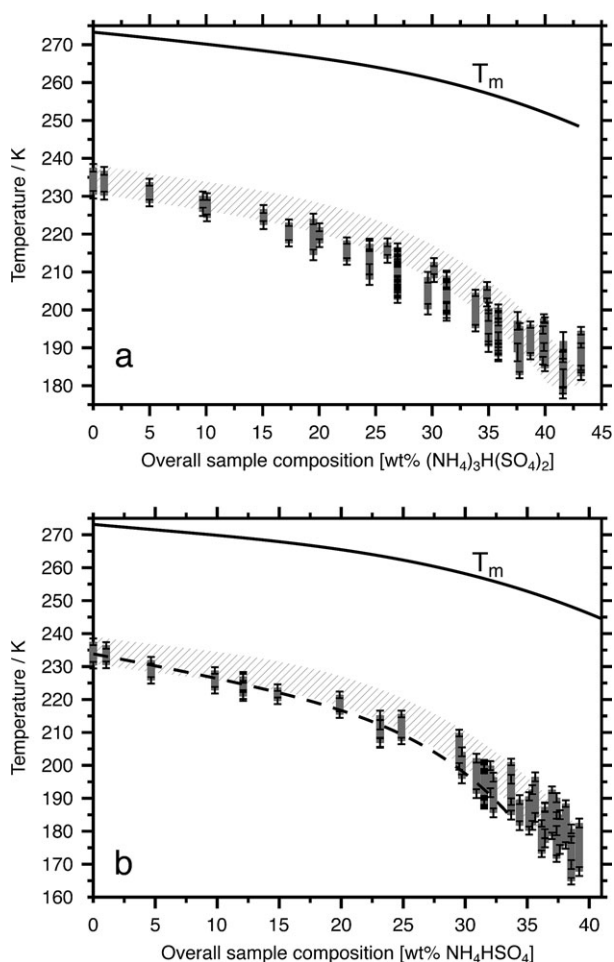


Fig. 6 Freezing temperatures of emulsified $(\text{NH}_4)_3\text{H}(\text{SO}_4)_2/\text{H}_2\text{O}$ (panel a) and $\text{NH}_4\text{HSO}_4/\text{H}_2\text{O}$ (panel b) solution droplets. The measured freezing temperature range, as the droplets were ramped down at a rate of 10 K min^{-1} , is shown by a solid grey bar; the uncertainty in freezing onset and completion are indicated. The ice melting temperature curve, as predicted by AIM,³² is also shown. In panel b, the dashed line is a polynomial fit to the mean freezing temperatures measured by Koop *et al.*,²⁷ in emulsified AHS solution droplets. The comparison with previous data is restricted to supermicron sized droplets—droplets of a similar size to those employed in the present study. The grey curve represents the freezing temperatures predicted by the water activity criterion for supermicron droplets^{46,47} and employing the thermodynamic model of Clegg *et al.*³² to predict water activity (see text for details).

measured where droplets fell through gas,^{39,42} suspended in an electrodynamic balance,⁴³ and suspended in oil emulsions.^{44,45} Our freezing results for the aqueous LET droplets, presented in Fig. 6a, are the first of their kind. This data adds to the growing body of data on the homogeneous freezing temperatures of ice in aqueous solution droplets.

We have also compared our measured ice freezing temperatures in Fig. 6 with those predicted by the water activity criterion model.^{46,47} Koop *et al.*⁴⁷ demonstrated that the homogeneous nucleation of ice in supercooled aqueous solution droplets only depends on the water activity of the solution ($a_w =$ ratio of the vapour pressure of the solution to that of pure water under the same conditions). They demonstrated

that the water activity at freezing (a_w^f) is equal to the water activity at the ice–liquid equilibrium (a_w^i) shifted to higher values by a constant offset (Δa_w), which was found to be 0.305 ($a_w^f = a_w^i + \Delta a_w$) for micron sized droplets. Koop⁴⁶ showed that most of the experimental data fell within 2.5% of the a_w^f line, and almost all of the data fall within 5%. We have plotted the prediction of the water activity criterion where Δa_w was set to 0.305 and the shaded region indicates the 2.5% deviation in a_w^f (the solute wt% corresponding to a_w^f was determined using AIM³² and a parameterisation of a_w^i was taken from Koop *et al.*⁴⁷). Inspection of Fig. 6 reveals that the homogeneous freezing of LET and AHS droplets is consistent with the water activity criterion.

Solute freezing temperatures in the aqueous solutions. The solute phase crystallisation temperatures are presented in Fig. 7 together with a parameterisation for the ice crystallisation temperatures. When letovicite crystallised it did so coincident with ice (within experimental uncertainties), whereas SAT in AHS droplets crystallised at around 178 K independently of solute concentration. Note that the full low-temperature scans between $2\theta = 19$ and 50° showed that small amounts of solute phase did crystallise outside the range of concentrations in which crystallisation itself was observed in Fig. 7, but the signal was too weak to reliably determine crystallisation temperatures during cooling. Approximately 15% of the total mass of the aqueous droplets must crystallise or melt in order to determine a phase change temperature. The results presented in Fig. 7 are the first measurements of the crystallisation temperature of solute phases in micron sized LET and AHS droplets that froze homogeneously. Koop *et al.*²⁷ used calorimetry to measure phase changes in bulk AHS solutions (volume = $3 \mu\text{L}$). In their bulk experiments ice nucleated heterogeneously, but the temperature at which SAT crystallised (181 K) was very similar to the present study (see Fig. 7b) even though ice nucleated at a much higher temperature.

Effect of aqueous solution composition and droplet size on the crystallisation of the solute

In this section we investigate the effect of the solution droplet composition (*i.e.* the solute : water mass ratio) and droplet size on solute crystallisation. In all of these experiments the emulsions were cooled down at a rate of 10 K min^{-1} to 173 K (or 163 K), at which point a diffraction pattern between $2\theta = 19$ to 50° was measured and the extent of crystallisation of the solute was determined from the diffraction patterns.

In order to provide a measure of the amount of crystalline solute that formed in the droplet after freezing, we determined the ratio of the intensity of a solute peak to the intensity of an ice peak. We refer to these intensity ratios as $I_{\text{solute}}/I_{\text{ice}}$. I_{solute} was divided by I_{ice} to remove any sample to sample variations in our data due to changes in sample thickness or sample volume probed by the X-ray diffractometer. In other words, division by I_{ice} provided a way to normalize the solute intensities. It should be noted that using just one peak to assess the amount of a particular material is not valid if the sample exhibits a preferred orientation, but as we demonstrated earlier this is not the case in our frozen emulsions.

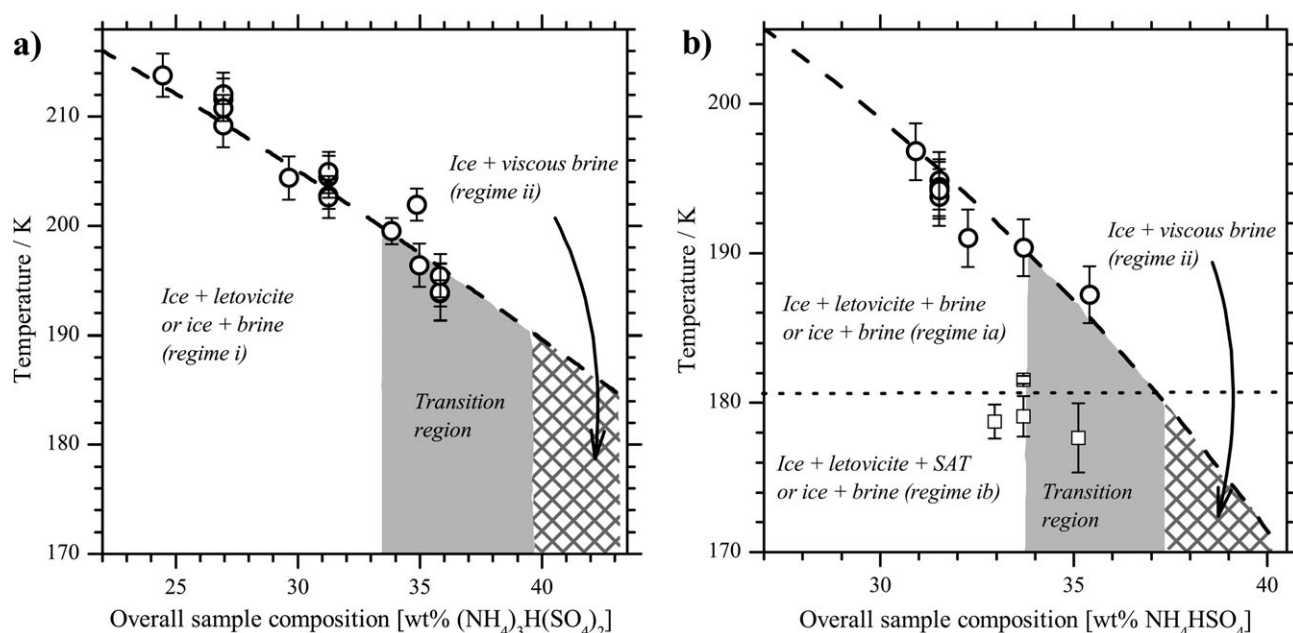


Fig. 7 Crystallisation temperatures of letovicite (circles) and SAT (squares) in the (a) $(\text{NH}_4)_3\text{H}(\text{SO}_4)_2/\text{H}_2\text{O}$ and (b) $\text{NH}_4\text{HSO}_4/\text{H}_2\text{O}$ systems. The dashed line is a parameterisation of the mean ice freezing temperatures shown in Fig. 6. The dotted line in a represents the SAT crystallisation temperature observed by Koop *et al.*²⁷ in their bulk experiments. The significance of regions *i*, *ii* ((a) and (b)) and the transition region are discussed in the text.

Hence the normalised intensity of a single peak is proportional to the amount of crystalline material. To quantify SAT and crystalline letovicite the diffraction peaks at $2\theta = 30$ and 31° were used, respectively. For normalization purposes, the ice peak at $2\theta = 40^\circ$ was used, which is a peak common to both hexagonal ice and cubic ice. The peak intensities were measured by fitting Gaussian profiles to the pertinent peaks in the diffraction patterns of frozen droplets, which were recorded at 173 K (or 163 K). The fitting procedure allowed us to deconvolute any overlap between peaks, although it should be borne in mind that peaks with minimal overlap were selected for this analysis. A similar analysis of diffraction patterns was used in the past.¹²

In Fig. 8 we have plotted $I_{\text{solute}}/I_{\text{ice}}$, as a function of the solute/water mass ratio ($M_{\text{solute}}/M_{\text{water}}$). Data for two size ranges, 2–5 μm and 10–20 μm bins are shown in Fig. 8. The 5–10 μm size range is omitted for clarity. These sizes refer to the volume median diameters which were determined for each emulsion sample using images of the droplets. Images were obtained with an optical microscope equipped with a digital camera.^{14,15}

A number of trends are clear from the data presented in Fig. 8. Firstly, there is a strong size dependence, with the solute phase showing a greater propensity to crystallise in larger droplets. In order to examine this size dependence in more detail we performed an additional series of experiments where the droplet size distribution was varied while holding the solution concentration constant (26.9 wt%, $M_{\text{solute}}/M_{\text{water}} = 0.37$, LET). The letovicite-ice intensity ratio ($I_{\text{solute}}/I_{40(\text{ice-common})}$; where the solute peak at 30° was used for SAT and that at 31° for LET) is plotted as a function of droplet volume median diameter (d_{vm}) in Fig. 9a; this plot clearly shows that less solute phase crystallises in small solu-

tion droplets. In fact, the size dependence was very strong when d_{vm} increased from 3 to 10 μm . The most likely explanation for this trend is that the nucleation rate of the solute phase is reduced substantially in smaller droplets. The rate of nucleation, whether heterogeneous, homogeneous, or pseudo-heterogeneous, is clearly reduced in the smaller droplets. The implications for these results to the atmosphere are discussed below (see the ‘Atmospheric implications’ section).

The second trend which is clear from Fig. 8 is that the amount of solute phase that crystallised on cooling droplets to 173 K decreased drastically above about 35 wt% ($M_{\text{solute}}/M_{\text{water}} = 0.54$) in both LET and AHS droplets. One might expect the amount of crystalline solute phase to increase with increasing mass fraction of solute; however this is clearly not the case. In fact, very little solute phase was detected in droplets of concentration greater than 39 wt% ($M_{\text{solute}}/M_{\text{water}} = 0.64$) AHS and 40 wt% ($M_{\text{solute}}/M_{\text{water}} = 0.67$) LET. Warming these concentrated solution droplets at a rate of 10 K min^{-1} results in crystallisation of the solute phase at around 189 and 186 K in LET and AHS, respectively (this only applies to the largest droplets where nucleation is efficient). This indicates that nucleation and/or crystal growth of the solute phase was limited at lower temperatures.

In the field of food technology and engineering, it is well known that crystallisation of the solute brine, post ice crystallisation, can be inhibited. In fact, considerable effort has been invested to find which ingredients may ‘stabilise’ the brine and prevent further alteration and crystallisation of frozen food products during storage.⁴⁸ When ice forms in aqueous solution, solute ions are rejected to form a brine. At equilibrium, this brine will have a unique concentration at a particular temperature which is determined by thermodynamics.³² However, in many cases the brine never reaches this equilibrium

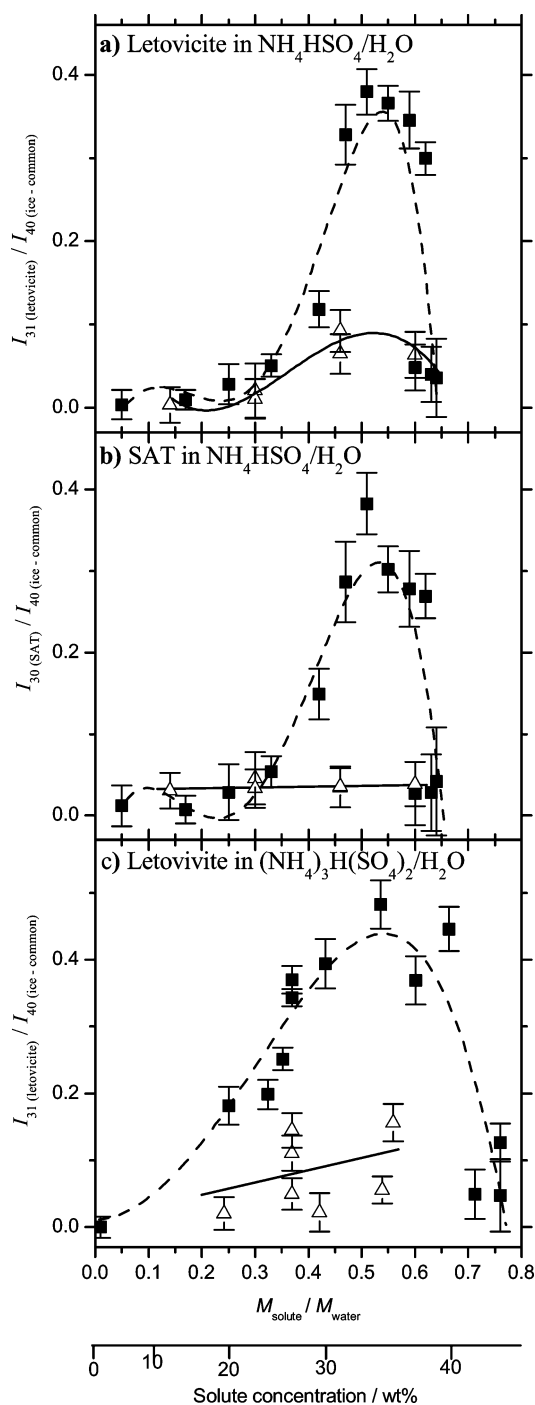


Fig. 8 The solute phase intensity ratios ($I_{\text{solute}}/I_{40(\text{ice-common})}$) as a function of solute to water mass ratio ($M_{\text{solute}}/M_{\text{water}}$). Data for droplets in the 10–20 μm (filled squares) and 2–5 μm (open triangles) droplet size ranges are plotted. (The size refers to the volume median diameter.) The intensity ratios I_{31}/I_{40} and I_{30}/I_{40} for letovicite and SAT, respectively, are plotted. The dashed and solid lines are fits to the data and are only intended to guide the eye.

with ice since the viscosity of aqueous solutions increases with both increasing concentration and decreasing temperature.^{48,49} This can result in the formation of mixtures of crystalline ice with highly viscous or even glassy material.⁴⁸ The experimental data presented here suggest that if ice forms

below a certain threshold temperature, the brine will rapidly become highly viscous and possibly form glassy material in which crystallisation is inhibited. In the next section we suggest that the formation of highly viscous amorphous brines may influence the phase of ice that results. Measurements of viscosity and glass transition temperatures for the pertinent solutions are highly desirable.

The relationship between ice phase and solute brine properties

Previous ice results. In our previous manuscript¹² we showed that the phase of ice that forms in LET and AHS droplets strongly depends on the ammonium to sulfate ratio (ASR) of the solute. This ice freezing data has been reproduced in Fig. 10a and c in order that it can be compared with the letovicite crystallisation data, which has been re-plotted in terms of ice freezing temperature rather than solution concentration. The phase of ice is indicated using the peak intensity ratio I_{44}/I_{40} , where I_{44} is the intensity of the peak at 44° exclusive to ice I_h and I_{40} is that of the common peak at 40° . A value of $I_{44}/I_{40} = 0.82 \pm 0.03$ indicates pure hexagonal ice formed and $I_{44}/I_{40} = 0$ indicates no bulk ice I_h formed and that the dominant product was ice I_c . The intensity ratios were determined from diffraction patterns measured at 173 K (or 163 K) after the droplets were cooled to this temperature at a rate of 10 K min^{-1} (see Murray and Bertram¹² for details). Note that these results were obtained from the same emulsions that were used in the experiments discussed above. Hence, the results from the ice studies are directly comparable to the results presented in this manuscript.

Here we briefly summarize our previous ice results for completeness. The plots in Fig. 10a and c highlight several important findings, including a strong solute type dependence and a significant size dependence at temperatures above ~ 200 K. Inspection of the sigmoidal fit through the 5–10 μm size bin, shown in Fig. 10d, reveals that for AHS there is no significant size dependence for the entire temperature range investigated. For LET solution compositions, there is no size dependence for temperatures less than ~ 200 K. At higher freezing temperatures there is evidence of a size dependence in the LET data, with larger droplets freezing to more ice I_c ; an opposite trend to that observed in pure water droplets.¹⁴ The trend observed previously for pure water is due to heating of the droplets during freezing. However, as discussed in our previous manuscript,¹² this is most likely not important for concentrated solution droplets; and indeed, one would expect an opposite size dependence if heating were important.

Perhaps the most important result illustrated in Fig. 10a and c is that the temperature below which cubic ice forms is strongly dependent on the solute type. For example, in LET droplets, the intensity ratios I_{44}/I_{40} is less than 0.2 at freezing temperatures below 200 ± 1 K (based on the fit to the freezing data), whereas for AHS droplets a value of 0.2 is not reached until below 183 ± 1 K. Uncertainties are based on the 95% confidence limit of the fit to the 5–10 μm size bin (Fig. 10).

Solute crystallisation and formation of highly viscous amorphous brines. From Fig. 10c and f we can identify several freezing temperature regimes based on the ability of the solute phase to crystallise. These approximate freezing temperature

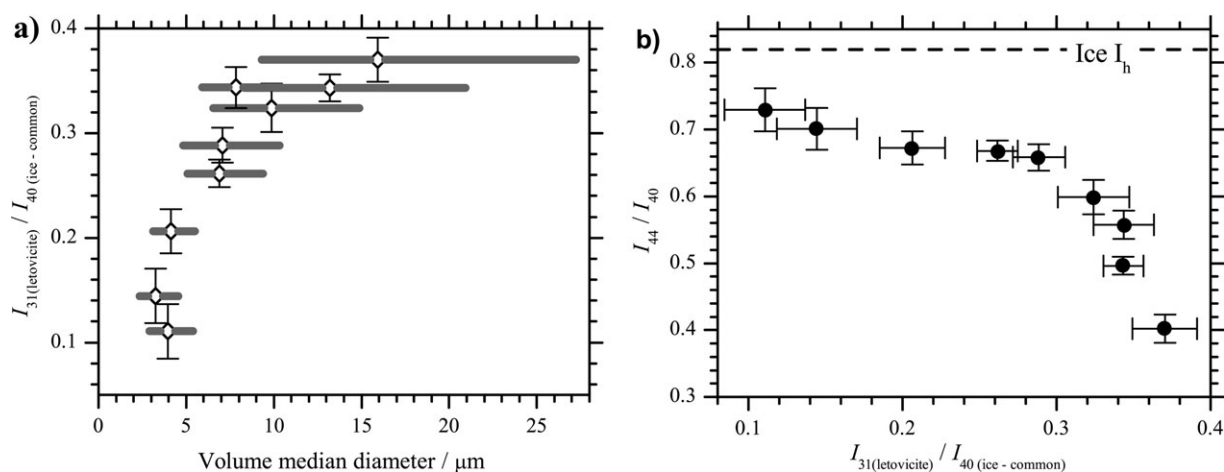


Fig. 9 (a) The letovicite–ice intensity ratio I_{31}/I_{40} (a measure of how much letovicite crystallised) plotted as a function of the volume median diameter for 26.9 wt% LET droplets. The droplet median diameter was determined from images taken with an optical microscope.^{12,15} The horizontal bars represent the size range in which 68% of the volume resides. (b) The ice I_h -common ice peak intensity ratio (I_{44}/I_{40}) as a function of letovicite ice intensity ratio, also with composition 26.9 wt% LET. A value of $I_{44}/I_{40} = 0.82 \pm 0.03$ indicates pure hexagonal ice formed and $I_{44}/I_{40} = 0$ indicates no bulk ice I_h formed and that the dominant product was ice I_c .

regimes are indicated in Fig. 10b and e. Temperature regime *i* is where there is an opportunity for crystallisation to take place before the droplets become highly viscous. In this regime nucleation and crystallisation took place in the largest droplets and crystallisation always took place coincident with ice crystallisation. This indicates that solute crystallisation took place as the ice crystals grew in the large droplets, but in the small droplets sufficient supersaturations for nucleation and crystallisation were not reached before the brine became highly viscous. In temperature regime *ii* the solute phase does not crystallise, most likely because the brine became highly viscous or glassy and crystal growth became very slow before crystallisation could take place. A transition region is also indicated where solute phase crystal growth was limited, but did occur to some measurable extent.

Inspection of Fig. 10 reveals that these regimes are correlated with the ice phase that forms. In regime *i*, where the ice spends some time in equilibrium with a mobile non-viscous brine, hexagonal ice results; whereas in regime *ii*, where the brine rapidly becomes highly viscous or glassy, cubic ice tends to result. In the following we suggest how the physical properties of the brine might influence the ice phase that we observe to form when aqueous droplets freeze.

Possible explanation of ice phase dependence on solute type.

In this section we attempt to rationalise our experimental results by considering the nucleation and crystallisation process in aqueous solution droplets. We start this discussion with nucleation and then outline how cubic ice might transform to hexagonal ice through a solvent mediated transformation. We suggest that it is this transformation which is critically influenced by the physical state and transport properties of the brine.

The empirical Ostwald's law of stages predicts that a metastable phase will initially form in preference to the stable phase.⁵⁰ In fact, there is substantial theoretical^{51–54} and ex-

perimental^{7,14,54–59} evidence that when aqueous droplets freeze, cubic ice preferentially nucleates and crystallises. Experimental evidence suggests that cubic ice may nucleate in droplets as high as 256 K^{58,60} and in a theoretical study Takahashi⁵¹ suggests that cubic ice may nucleate below 271 K. This can be rationalised with the classical nucleation theory which predicts that the free energy associated with the production of a critical embryo, ΔG^* is

$$\Delta G^* = \frac{16\pi\gamma^3\nu^2}{3(kT \ln S)^2} \quad (1)$$

where γ is the surface free energy between the ice germ and the supercooled liquid, ν is the molecular volume, k is Boltzmann's constant, T is temperature and S is the saturation ratio. In an elegant experiment Huang and Bartell⁵⁹ demonstrated that γ for a germ of ice I_c is substantially smaller than for ice I_h . The height of the energy barrier is strongly influenced by γ , due to the cubic term. Since the rate at which critical germs form, J is thought to be proportional to $\exp(-\Delta G^*/kT)$, the nucleation of critical germs of ice I_c will be favoured over the nucleation of hexagonal critical germs. Assuming that the cubic germ then acts as a template for subsequent ice layers, cubic ice will crystallise as the dominant product.

We know from calorimetry¹¹ and vapour pressure measurements¹⁰ that ice I_c is metastable to ice I_h and theoretical work suggests this is the case from 0 to 273 K at atmospheric pressure.⁶¹ Ice I_c therefore has a larger chemical potential than ice I_h :

$$\mu_{I_c} > \mu_{I_h} \quad (2)$$

Therefore, the transition of ice I_c to ice I_h is thermodynamically favourable. If ice I_c is to persist, as it does in our experiments, there must be kinetic limitations to this transformation. In the following we list the potential mechanisms through which the cubic to hexagonal transformation might

occur: Firstly, there is a gas phase route, which is active in vapour deposited ice I_c samples. In this mechanism cubic and hexagonal ice share a common vapour phase and since cubic ice has a larger vapour pressure than hexagonal ice (since $\mu_c > \mu_h$),^{10,11,62} mass transfer of water molecules from cubic to hexagonal particles will occur.¹¹ This becomes rapid (minutes) above about 200 K.¹¹ It is this mechanism through which Murphy¹¹ has suggested cold ice clouds might be influenced by

the transient presence of cubic particles. The vapour phase is not accessible to the droplets in the experiments described here, since they are locked in an oil matrix. Secondly, there is a bulk solid-to-solid transformation, but it has been previously shown that this mechanism does not become rapid in micrometer sized pure water droplets until above ~ 240 K.¹⁴ Hence, this mechanism is most likely not important when droplets crystallise well below 240 K, and remain below 240 K as in the current experiments.

In addition to the gas-phase mass transfer and solid-to-solid mechanisms there may be a third transformation mechanism that operates when ice forms in aqueous solution droplets. This is a solvent-mediated cubic-to-hexagonal transition, where water molecules travel from a cubic crystal to a hexagonal crystal *via* the aqueous brine. Solvent-mediated transformations are known to be important in other systems,⁵⁰ but to the best of our knowledge have not been discussed in the past specifically for ice. Clearly, if cubic ice initially forms, the nature of the brine will therefore play a critical role in determining the final phase of ice. Cubic ice will only be stabilized if the brine crystallises or if the brine is highly viscous. Based on this, one would expect to see a correlation between our solute crystallisation results and the ice results. We now show that this solvent mediated phase transformation is a physically reasonable mechanism in droplets where ice forms, but where the brine is non-viscous.

The solvent mediated phase transformation requires both ice I_c and ice I_h to be present within the same droplets. In fact, this is very likely. Murphy¹¹ points out that the (111) face of ice I_c is very similar to the (1000) face of ice I_h , hence the barrier to nucleation of ice I_h on ice I_c should therefore be small. So a situation likely exists where both ice I_c and ice I_h are in contact with an aqueous brine. Thermodynamics dictates that the more stable phase (*i.e.* lower chemical potential) will always have a lower solubility in any given solvent. Hence, the concentration of water in the aqueous solution immediately above ice I_c will be larger than the concentration of water above ice I_h crystals ($C_{w,I_c} > C_{w,I_h}$). This will give rise to concentration gradients in the aqueous brine between regions of ice I_c and ice I_h . Consequently the ice I_h crystals will tend to grow at the expense of the ice I_c crystals at a rate which may be dictated by Fick's first law of diffusion.⁶³ The rate at which water molecules diffuse from cubic regions to hexagonal

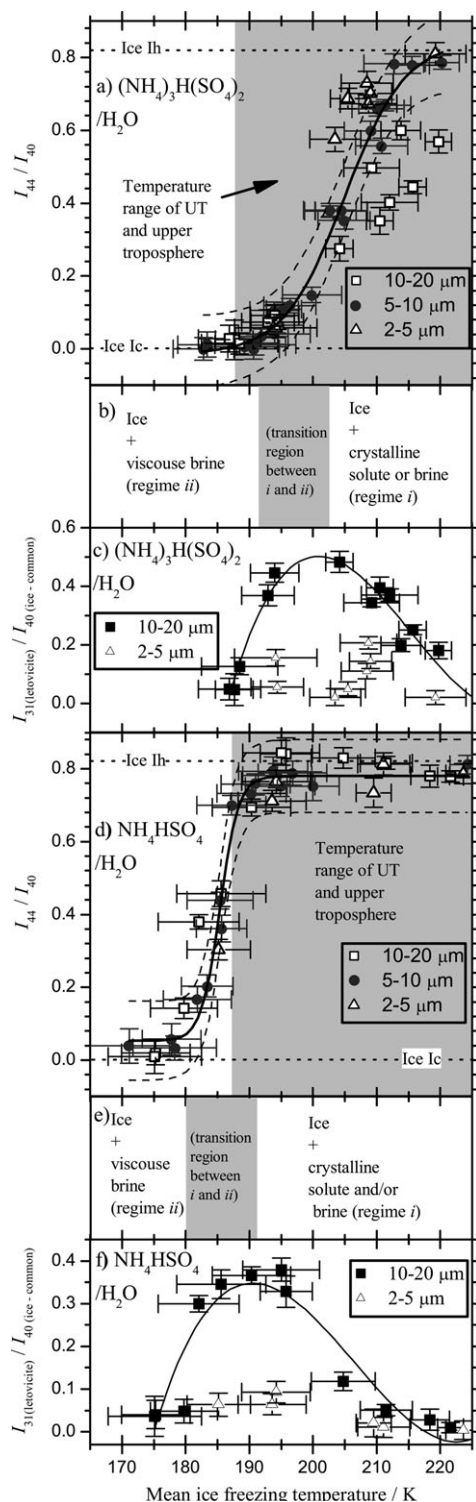


Fig. 10 The ice I_h -common ice peak intensity ratio, I_{44}/I_{40} , and the letovcite-ice intensity ratio, I_{31}/I_{40} , as a function of mean ice freezing temperature for AHS and LET in droplets that were cooled from room temperature to 173 K at a rate of 10 K min^{-1} . I_{44}/I_{40} is shown for three size ranges in LET (a) and AHS d solution droplets. The solid line in panels a and d are sigmoidal fits to the 5–10 μm data and the dotted lines are the corresponding 95% prediction bands. Uncertainties in the mean freezing temperature are indicated. In panels c and f, the ratio I_{31}/I_{40} is shown as a function of the temperature at which ice formed in the droplets in order to compare the crystallisation of the solute phase with the phase of ice that formed. Data for the larger and smaller size ranges are shown; the middle size range is excluded for clarity. Panels b and e refer to the state of the droplet after ice formed and it had been cooled to 173 K and are discussed in detail in the text. The regimes *i* and *ii* correspond to the regimes marked in Fig. 7.

regions, W , can be expressed:

$$W = -D \frac{dC}{dx} \quad (3)$$

where x is distance, hence the differential is the concentration gradient of water in the aqueous brine between regions of solution near ice I_c to regions near ice I_h , and D is the diffusion coefficient of water in the aqueous brine. D is approximately inversely proportional to viscosity.⁵⁰ Consequently, the rate at which a solvent mediated phase transformation takes place will be strongly dependent on the viscosity of the brine. Intriguingly, measurements in supercooled sulfuric acid solutions show that viscosity increases dramatically as temperature falls and concentration of sulfuric acid increases.⁶⁴ In fact, many aqueous solutions exhibit a super-Arrhenius dependence of viscosity on temperature.⁶⁵ For example, Maltini and Anese⁴⁹ estimate that the combined effect of increasing con-

centration and decreasing temperature on a sucrose solution cooled from -10 to -20 °C results in an increase in viscosity by a factor of $\sim 10^5$. Unfortunately, no measurements for transport properties exist for LET or AHS solutions under pertinent conditions but it is reasonable to expect that D will decrease dramatically with decreasing T and increasing concentration. We suggest that the solvent-mediated phase transformation can become limited shortly after ice forms and the solute is rejected from the growing cubic ice crystal to form a more concentrated, more viscous brine. We also suggest that this may provide an explanation for the dependence of ice phase on droplet ASR since transport properties in aqueous solution are dependent on the physical properties of the solute.⁶⁵

Experimental evidence for a solvent mediated cubic to hexagonal ice phase transition. Let us first consider the phase of ice

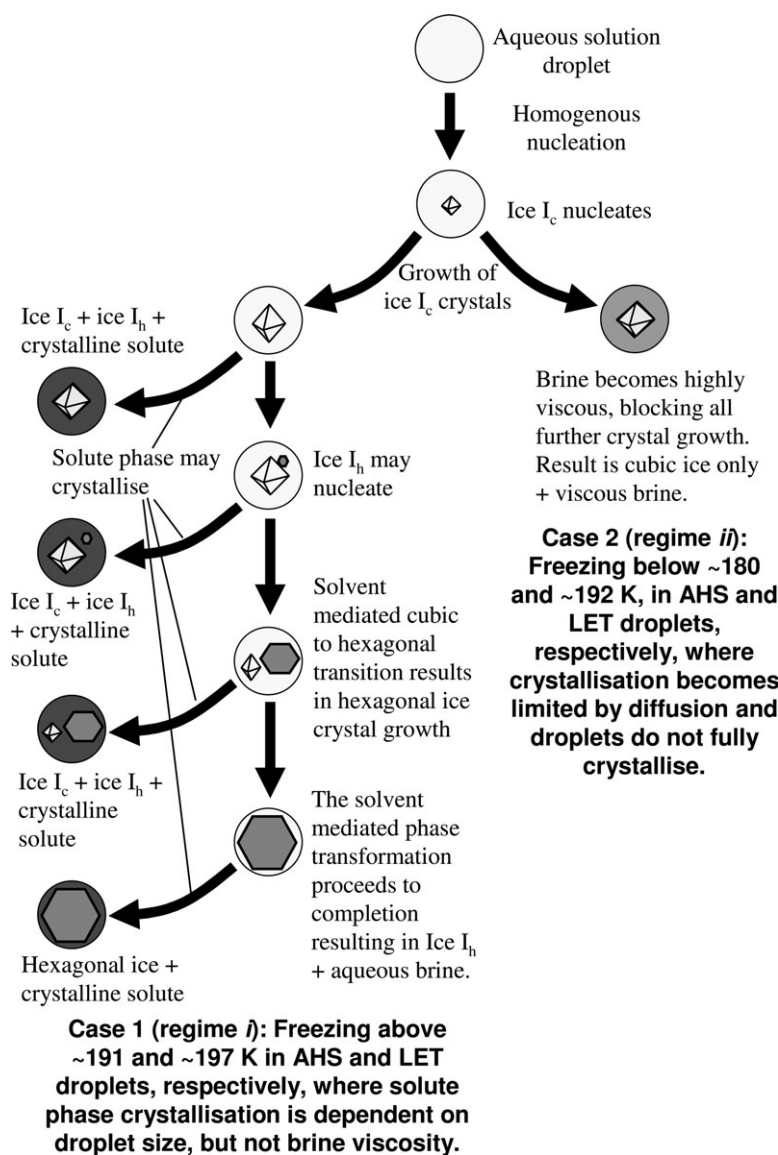


Fig. 11 Flow diagram illustrating the crystallisation pathways a supercooled aqueous droplet might take when ice homogeneously nucleates within it. The octahedron represents an octahedral crystal of cubic ice, and the hexagon represents hexagonal ice crystals. Note that crystallisation in real droplets most likely results in many crystallites formed through dendritic growth.¹⁹

that formed in LET droplets in temperature regime *i*. Recall that the crystallisation of letovicite is droplet size dependent (see Fig. 9), which indicated that nucleation and crystallisation in this regime were not limited by diffusion in the brine, but rather by nucleation. If the solvent-mediated cubic-to-hexagonal transition is active in determining the final phase of ice then one would expect more cubic ice in droplets where letovicite crystallised more readily, *i.e.* the larger droplets. In order to test this hypothesis we performed a series of experiments with a solution of 26.9 wt% LET, where we varied the droplet size. In Fig. 9b we plot the ratio of I_{44}/I_{40} vs. our measure of the amount of letovicite that crystallised, $I_{31(\text{letovicite})}/I_{40(\text{ice-common})}$, and shows that ice I_c is stabilised in the case where more letovicite crystallised. These data are consistent with our postulated solvent mediated phase transformation.

In the case of AHS in regime *i*, the solute phase crystallises more readily in larger droplets, as it does in LET droplets. However, the situation is complicated by the fact that a brine always persists on cooling to about 178 K, the measured SAT crystallisation temperature (even in the largest droplets). Hence, in any droplets in which ice forms above 178 K, the ice will spend some time in contact with a brine until SAT crystallises, thus the crystallisation of letovicite alone is not sufficient to block the solvent mediated transformation. Hence we would predict that hexagonal ice would dominate in the regime where letovicite can crystallise and that there would be no size dependence of ice phase (regime *i*). Inspection of Fig. 10 reveals that hexagonal ice does indeed dominate in this region for all droplet sizes.

We will now consider regime *ii*, where the crystallisation of the solute phase was strongly limited. Earlier in this paper it was argued that the brine which forms after ice has crystallised was highly viscous and diffusion of water and ions was very slow. In this case we would expect to see cubic ice as the main product based on the nucleation kinetics and solvent mediated transformation discussed above. It is clear from Fig. 10 that cubic ice does dominate in this regime *ii*.

The flow diagram in Fig. 11 is designed to illustrate the crystallisation pathways that a freezing droplet may take. When ice nucleates in a supercooled aqueous solution droplet there are a number of potential routes. In the first case, which corresponds to droplets in regime *i*, cubic ice nucleates and grows and is in contact with aqueous brine. Hence, a solvent-mediated phase transformation will be active unless the solute phase(s) completely crystallise. The final mixture of ice I_c and ice I_h is determined by how efficiently the solute phase nucleates and crystallises. Our results show that letovicite is more likely to crystallise in a 20 μm LET droplet than in a 1 μm LET droplet, and hence the solvent mediated transition would have less time to operate and cubic ice would be more likely to dominate. On the other hand, in AHS droplets a brine would exist even if letovicite crystallised, thus providing a medium for the solvent mediated phase transformation. Atmospheric aerosols are often complex internal mixtures, hence a brine would often exit and if in regime *i*, hexagonal ice would most likely result. Alternatively, the droplets may be in regime *ii* (case 2), where ice I_c nucleates and crystallises, but as the ice crystals grow the brine becomes increasingly viscous as its

concentration increases and its temperature decreases. This results in partially crystallised droplets which contain cubic ice that is stabilised, and a highly viscous or glassy brine in which solute crystallisation is limited. We suggest that the formation of these internally mixed cubic ice and highly viscous brines may form in the atmosphere and may influence cloud formation and properties.

Summary and atmospheric implications

For the first time we have directly identified the phases that form in LET and AHS solution droplets after ice homogeneously nucleates. When LET droplets crystallise we find that letovicite II, rather than the expected letovicite III,²⁸ forms. In AHS droplets we find that a distorted letovicite II forms in addition to SAT, whereas letovicite III and SAH might have been expected.^{28,32} These results illustrate how useful X-ray diffraction is in determining the phases that crystallise from highly supercooled atmospherically relevant solution droplets.

In addition to determining phases that form, we also determine how much of the solute phases crystallise as a function of droplet size, solute type and solute concentration. We have shown that the crystallisation of the solute phase is strongly size dependent and is limited in droplets of less than $\sim 5 \mu\text{m}$. Atmospheric droplets that freeze to form cirrus cloud ice particles tend to be in the sub-micrometer size range; hence, our results suggest that crystallisation of the solute phase may be strongly limited in many atmospheric droplets. However, it is likely that the crystallisation of the solute phase also depends on time. In our experiments the time for crystallisation is short and it may be much longer in the atmosphere. More work is required to determine the effect of time. If the brine does not crystallise then homogeneous freezing cannot directly contribute to a population of solid salt particles. It has been suggested that these particles catalyse ice formation in subsequent cloud cycles.^{18–23} Our results suggest that the dominant production mechanism for solid salt particles is *via* efflorescence, which is thought to be an important process in the atmosphere.^{66,67} In addition, Bogdan *et al.*¹⁷ suggest that an ‘overlayer’ of liquid brine on ice crystals may influence heterogeneous chemistry, optical properties and ice crystal growth kinetics of low temperature ice clouds.

In more concentrated solution droplets the crystallisation of the solute phase in all droplets, including the largest ones (10–20 μm), is limited below freezing temperatures of 192 and 180 K in $(\text{NH}_4)_3\text{H}(\text{SO}_4)_2$ and NH_4HSO_4 , respectively. The most likely explanation for this behaviour is that the brine which forms below these freezing temperatures becomes highly viscous, thus dramatically reducing the crystal growth rate of any nucleated solute crystals.

The inhibition of crystallisation of the solute phase in low temperature brines has led us to propose that the phase of ice that forms in solution droplets is determined by a solvent-mediated cubic-to-hexagonal phase transformation. Hence the nature of the aqueous brine can strongly influence the final phase of ice and therefore provides an explanation for the strong solute dependence of ice phase observed in our previous study.¹² At higher freezing temperatures the solvent-mediated

transformation is only blocked if the solute crystallises; if it is not blocked hexagonal ice results, whereas below some threshold freezing temperatures the transformation is effectively blocked when the brine becomes highly viscous and cubic ice is therefore the dominant crystalline product. We have shown strong differences when simply changing the ASR of droplets from 1.5 to 1.0, which presumably reflects the physical properties of the brine. Glass transition temperatures and viscosity of pertinent aqueous solutions need to be experimentally determined in order to test the proposed solvent mediated phase transformation. In addition it should also be noted that real atmospheric droplets are often more complex than the model systems employed here, often containing organics and nitrates amongst other species. The impact of these other chemical species needs to be examined in future laboratory studies.

Acknowledgements

The authors thank Dr Christoph Salzmann (Oxford University) for very helpful advice on refining structures and employing the Rietveld method. We also gratefully acknowledge A. Lam and B. Patrick (UBC) for assistance with X-ray diffraction measurements. This work was funded by the Natural Science and Engineering Research Council of Canada, NSERC, the Canadian Foundation for Climate and Atmospheric Sciences, CFCAS, and the Canada Foundation for Innovation, CFI. BJM gratefully acknowledges the Natural Environmental Research Council, NERC, for a fellowship (NE/D009308/1) held at the School of Chemistry, University of Leeds, which commenced in September 2006.

References

- D. K. Lynch, in *Cirrus*, ed. D. K. Lynch, K. Sassen, D. C. Starr and G. Stephens, Oxford University Press, Oxford, 2002, p. 1.
- K. Sassen, in *Cirrus*, ed. D. K. Lynch, K. Sassen, D. C. Starr and G. Stephens, Oxford University Press, Oxford, 2002, p. 11.
- K. L. Denman, G. Brasseur, A. Chidthaisong, P. Ciais, P. M. Cox, R. E. Dickinson, D. Hauglustaine, C. Heinze, E. Holland, D. Jacob, U. Lohmann, S. Ramachandran, P. L. da Silva Dias, S. C. Wofsy and X. Zhang, in *Climate Change 2007: The Physical Science Basis. Contribution of Working Group I to the Fourth Assessment Report of the Intergovernmental Panel on Climate Change*, ed. S. Solomon, D. M. Qin, Z. Manning, M. Chen, K. B. Marquis, M. T. Averyt and H. L. Miller, Cambridge University Press, Cambridge, 2007.
- E. Jensen and L. Pfister, *Geophys. Res. Lett.*, 2005, **32**, D03208.
- O. B. Toon, R. P. Turco, J. Jordan, J. Goodman and G. Ferry, *J. Geophys. Res.*, [Atmos.], 1989, **94**, 11359.
- P. J. DeMott, in *Cirrus*, ed. D. K. Lynch, K. Sassen, D. C. Starr and G. Stephens, Oxford University Press, Oxford, 2002, p. 102.
- B. J. Murray, D. A. Knopf and A. K. Bertram, *Nature*, 2005, **434**, 202.
- H. Grothe, H. Tizek, D. Waller and D. J. Stokes, *Phys. Chem. Chem. Phys.*, 2006, **8**, 2232.
- H. R. Pruppacher and J. D. Klett, *Microphysics of Clouds and Precipitation*, Kluwer, Dordrecht, 1997.
- J. E. Shilling, M. A. Tolbert, O. B. Toon, E. J. Jensen, B. J. Murray and A. K. Bertram, *Geophys. Res. Lett.*, 2006, **33**, L17801.
- D. M. Murphy, *Geophys. Res. Lett.*, 2003, **30**, 2230.
- B. J. Murray and A. K. Bertram, *Geophys. Res. Lett.*, 2007, **34**, L16810.
- X. L. Zhou, M. A. Geller and M. H. Zhang, *J. Climate*, 2004, **17**, 2901.
- B. J. Murray and A. K. Bertram, *Phys. Chem. Chem. Phys.*, 2006, **8**, 186.
- B. J. Murray and A. K. Bertram, in *Physics and Chemistry of Ice*, ed. W. F. Kuhs, The Royal Society of Chemistry, Cambridge, 2007, p. 417.
- T. Koop, A. Kapilashrami, L. T. Molina and M. J. Molina, *J. Geophys. Res.*, [Atmos.], 2000, **105**, 26393.
- A. Bogdan, M. J. Molina, K. Sassen and M. Kulmala, *J. Phys. Chem. A*, 2006, **110**, 12541.
- B. Zobrist, C. Marcolli, T. Koop, B. P. Luo, D. M. Murphy, U. Lohmann, A. A. Zardini, U. K. Krieger, T. Corti, D. J. Cziczo, S. Fueglistaler, P. K. Hudson, D. S. Thomson and T. Peter, *Atm. Chem. Phys.*, 2006, **6**, 3115.
- B. Zuberi, A. K. Bertram, T. Koop, L. T. Molina and M. J. Molina, *J. Phys. Chem. A*, 2001, **105**, 6458.
- J. P. D. Abbatt, S. Benz, D. J. Cziczo, Z. Kanji, U. Lohmann and O. Mohler, *Science*, 2006, **313**, 1770.
- J. E. Shilling, T. J. Fortin and M. A. Tolbert, *J. Geophys. Res.*, [Atmos.], 2006, **111**, D12204.
- A. Tabazadeh and O. B. Toon, *Geophys. Res. Lett.*, 1998, **25**, 1379.
- M. Baker, *Nature*, 2001, **413**, 586.
- K. D. Beyer and J. Bothe, *J. Phys. Chem. A*, 2006, **110**, 7105.
- K. D. Beyer, J. Bothe and N. Burmann, *J. Phys. Chem. A*, 2007, **111**, 479.
- K. D. Beyer, A. R. Hansen and M. Poston, *J. Phys. Chem. A*, 2003, **107**, 2025.
- T. Koop, A. K. Bertram, L. T. Molina and M. J. Molina, *J. Phys. Chem. A*, 1999, **103**, 9042.
- S. Martin, *Chem. Rev.*, 2000, **100**, 3403.
- K. Gesi, *Phys. Status Solidi A*, 1976, **33**, 479.
- P. M. Dominiak, J. Herold, W. Kolodziejski and K. Wozniak, *Inorg. Chem.*, 2003, **42**, 1590.
- W. Kraus and G. Nolze, *J. Appl. Crystallogr.*, 1996, **29**, 301.
- S. L. Clegg, P. Brimblecombe and A. S. Wexler, *J. Phys. Chem. A*, 1998, **102**, 2137.
- A. D. Fortes, I. G. Wood, L. Vočadlo, L. Chapon, K. S. Knight and R. I. Smith, *J. Chem. Phys.*, 2008, **128**, , DOI: 10.1063/1.2827474.
- D. Mootze and A. Merschenz-Quack, *Z. Naturforsch.*, 1987, **42B**, 1231.
- R. A. Young, *The Rietveld Method*, Oxford University Press, New York, 1993.
- A. Goto, T. Hondoh and S. Mae, *J. Chem. Phys.*, 1990, **93**, 1412.
- D. G. Imre, J. Xu, I. N. Tang and R. McGraw, *J. Phys. Chem. A*, 1997, **101**, 4191.
- J. H. Chelf and S. T. Martin, *Geophys. Res. Lett.*, 1999, **26**, 2391.
- B. H. Larson and B. D. Swanson, *J. Phys. Chem. A*, 2006, **110**, 1907.
- A. K. Bertram, T. Koop, L. T. Molina and M. J. Molina, *J. Phys. Chem. A*, 2000, **104**, 584.
- H. Y. A. Chang, T. Koop, L. T. Molina and M. J. Molina, *J. Phys. Chem. A*, 1999, **103**, 2673.
- S. E. Wood, M. B. Baker and B. D. Swanson, *Rev. Sci. Instrum.*, 2002, **73**, 3988.
- P. Stockel, I. M. Weidinger, H. Baumgartel and T. Leisner, *J. Phys. Chem. A*, 2005, **109**, 2540.
- P. Taborek, *Phys. Rev. B*, 1985, **32**, 5902.
- D. H. Rasmussen and A. P. MacKenzie, *J. Chem. Phys.*, 1973, **59**, 5003.
- T. Koop, *Z. Phys. Chem.*, 2004, **218**, 1231.
- T. Koop, B. P. Luo, A. Tsias and T. Peter, *Nature*, 2000, **406**, 611.
- D. S. Reid, W. Kerr and J. Hsu, *J. Food Eng.*, 1994, **22**, 483.
- E. Maltini, M. Anese and I. Shtylla, *Cryo-Letters*, 1997, **18**, 263.
- J. W. Mullin, *Crystallization*, Elsevier Butterworth-Heinemann, Oxford, 2001.
- T. Takahashi, *J. Cryst. Growth*, 1982, **59**, 441.
- H. Kieft, M. J. Clouter and E. Whalley, *J. Chem. Phys.*, 1984, **81**, 1419.
- I. M. Svishchev and P. G. Kusalik, *Phys. Rev. Lett.*, 1994, **73**, 975.
- L. S. Bartell and Y. G. Chushak, in *Water in Confined Geometries*, ed. V. Buch and J. P. Devlin, Springer-Verlag, Berlin, 2003, p. 399.
- E. Mayer and A. Hallbrucker, *Nature*, 1987, **325**, 601.
- I. Kohl, E. Mayer and A. Hallbrucker, *Phys. Chem. Chem. Phys.*, 2000, **2**, 1579.
- Y. Furukawa, *J. Meteorol. Soc. Jpn.*, 1982, **60**, 535.
- H. Uyeda and K. Kikuchi, *J. Meteorol. Soc. Jpn.*, 1976, **54**, 267.
- J. F. Huang and L. S. Bartell, *J. Phys. Chem.*, 1995, **99**, 3924.

-
- 60 H. Uyeda and K. Kikuchi, *J. Meteorol. Soc. Jpn.*, 1980, **58**, 52.
61 H. Tanaka, *J. Chem. Phys.*, 1998, **108**, 4887.
62 A. Kouchi, *Nature*, 1987, **330**, 550.
63 P. W. Atkins, *Physical Chemistry*, Oxford University Press, Oxford, 1990.
64 L. R. Williams and F. S. Long, *J. Phys. Chem.*, 1995, **99**, 3748.
65 C. A. Angell, *Chem. Rev.*, 2002, **102**, 2627.
66 C. A. Colberg, U. K. Krieger and T. Peter, *J. Phys. Chem. A*, 2004, **108**, 2700.
67 C. A. Colberg, B. P. Luo, T. Koop and T. Peter, *Atmos. Chem. Phys.*, 2003, **3**, 909.
68 Y. Yao, M. Massucci, S. L. Clegg and P. Brimblecombe, *J. Phys. Chem. A*, 1999, **103**, 3678.